AMERICAN SOCIETY FOR MICROBIOLOGY | Journal of Virology®

Mutagenic Analysis of Hazara Nairovirus Nontranslated Regions during Single- and Multistep Growth Identifies both Attenuating and Functionally Critical Sequences for Virus Replication

Daniele F. Mega,[a] Jack Fuller,[a] Beatriz Álvarez-Rodríguez,[a] Jamel Mankouri,[a] Roger Hewson,[b] John N. Barr[a]

[a]School of Molecular and Cellular Biology, University of Leeds, Leeds, United Kingdom
[b]National Infection Service, Public Health England, Porton Down, Salisbury, United Kingdom

ABSTRACT Hazara nairovirus (HAZV) is a member of the family *Nairoviridae* in the order *Bunyavirales* and closely related to Crimean-Congo hemorrhagic fever virus, which is responsible for severe and fatal human disease. The HAZV genome comprises three segments of negative-sense RNA, named S, M, and L, with nontranslated regions (NTRs) flanking a single open reading frame. NTR sequences regulate RNA synthesis and, by analogy with other segmented negative-sense RNA viruses, may direct activities such as virus assembly and innate immune modulation. The terminal-proximal nucleotides of 3′ and 5′ NTRs exhibit extensive terminal complementarity; the first 11 nucleotides are strictly conserved and form promoter element 1 (PE1), with adjacent segment-specific nucleotides forming PE2. To explore the functionality of NTR nucleotides within the context of the nairovirus multiplication cycle, we designed infectious HAZV mutants bearing successive deletions throughout both S segment NTRs. Fitness of rescued viruses was assessed in single-step and multistep growth, which revealed that the 3′ NTR was highly tolerant to change, whereas several deletions of centrally located nucleotides in the 5′ NTR led to significantly reduced growth, indicative of functional disruption. Deletions that encroached upon PE1 and PE2 ablated virus growth and identified additional adjacent nucleotides critical for viability. Mutational analysis of PE2 suggest that its signaling ability relies solely on interterminal base pairing and is an independent *cis*-acting signaling module. This study represents the first mutagenic analysis of nairoviral NTRs in the context of the infectious cycle, and the mechanistic implications of our findings for nairovirus RNA synthesis are discussed.

IMPORTANCE Nairoviruses are a group of RNA viruses that include many serious pathogens of humans and animals, including one of the most serious human pathogens in existence, Crimean-Congo hemorrhagic fever virus. The ability of nairoviruses to multiply and cause disease is controlled in major part by nucleotides that flank the 3′ and 5′ ends of nairoviral genes, called nontranslated regions (NTRs). NTR nucleotides interact with other virus components to perform critical steps of the virus multiplication cycle, such as mRNA transcription and RNA replication, with other roles being likely. To better understand how NTRs work, we performed the first comprehensive investigation of the importance of NTR nucleotides in the context of the entire nairovirus replication cycle. We identified both dispensable and critical NTR nucleotides, as well as highlighting the importance of 3′ and 5′ NTR interactions in virus growth, thus providing the first functional map of the nairovirus NTRs.

KEYWORDS attenuation, genetics, Hazara, nontranslated regions, promoters, replication, rescue, reverse, virus

Citation Mega DF, Fuller J, Álvarez-Rodríguez B, Mankouri J, Hewson R, Barr JN. 2020. Mutagenic analysis of Hazara nairovirus nontranslated regions during single- and multistep growth identifies both attenuating and functionally critical sequences for virus replication. J Virol 94:e00357-20. https://doi.org/10.1128/JVI.00357-20.

Editor Rebecca Ellis Dutch, University of Kentucky College of Medicine

Address correspondence to John N. Barr, j.n.barr@leeds.ac.uk.

Received 28 February 2020
Accepted 2 May 2020
Accepted manuscript posted online 10 June 2020
Published 17 August 2020

The order *Bunyavirales* encompasses a diverse collection of over 500 segmented, enveloped RNA viruses that infect a broad range of hosts, including humans, animals, insects, and plants. The family *Nairoviridae* is one of 12 families in this order, which currently includes 12 distinct species (1). Nairoviruses are tick-borne, being specifically associated with hard ticks of the family *Ixodidae*, with transmission to mammalian and avian hosts occurring through acquisition of a blood meal. Nairoviruses are the causative agents of serious or fatal disease in animals, with humans representing dead-end hosts. The family is named after Nairobi sheep disease virus (NSDV), which causes disease in susceptible goats and sheep that carries a case fatality rate of around 80% and results in considerable economic impact (2). Crimean-Congo hemorrhagic fever virus (CCHFV) is a nairovirus of great clinical importance, responsible for a devastating disease in humans known as Crimean-Congo hemorrhagic fever (CCHF), which exhibits a case fatality rate of around 30%, rising to 80% in specific outbreaks (3). Concerns are growing over the spread and emergence of CCHFV due to the changing habitat of the tick vector in response to climate change, a threat confirmed by the recent cases of CCHF in northern Spain (4). Due to the severe outcome of CCHFV infection, paired with the lack of options for treatment or prevention of CCHF, this virus is one of a select group of human pathogens classified in hazard group 4 by the Advisory Committee on Dangerous Pathogens (Department of Health, United Kingdom). In contrast, Hazara nairovirus (HAZV) is not associated with human disease, despite being closely related to CCHFV and sharing the same CCHFV serogroup in the family *Nairoviridae*, as well as structural and functional properties (5–7). In view of the lack of HAZV-associated human disease, this virus can be handled under relatively unrestrictive biosafety level 2 (BSL-2) containment protocols. HAZV represents a valuable model system with which to gain knowledge of the nairovirus multiplication cycle.

All nairoviruses possess a trisegmented negative stranded RNA genome and share a genetic organization: the three genomic segments are named small (S), medium (M), and large (L) based on their relative sizes, and each acts as the template for transcription of a single mRNA. The S segment mRNA encodes the major nucleocapsid protein (N), the M segment mRNA encodes a glycosylated polyprotein precursor (GPC) that is cleaved into envelope spike proteins Gn and Gc, and the L segment mRNA encodes the RNA-dependent RNA polymerase (RdRp) responsible for transcription and replication of the three RNA segments. An additional open reading frame (ORF) in the CCHFV S segment, accessed by ambisense transcription of its antigenome, has been reported to express a nonstructural protein, NSs, with a role in modulating apoptosis (8), and the cleavage of Gn and Gc moieties from the M segment-specific polyprotein is predicted to yield a polypeptide that may represent the nonstructural protein NSm.

By analogy with other bunyaviruses, the RNA synthesis activities of the three nairovirus RNA segments are predicted to be controlled by nucleotide sequences within 3′ and 5′ nontranslated regions (NTRs), which flank the S, M, and L ORFs. Of all the members of the order *Bunyavirales*, perhaps the best studied in terms of the mechanism of RNA synthesis are Bunyamwera virus (BUNV) and La Crosse virus (LACV) of the family *Peribunyaviridae*, for which a combination of functional (9–18) and structural (19) studies have elucidated roles for individual nucleotides from within their respective NTRs. The terminal nucleotides of 3′ and 5′ NTRs exhibit terminal complementarily, and such sequences have been shown to bind to, and influence the activity of, the viral RdRp (19), promoting primer-dependent transcription to yield a 5′-capped mRNA, as well as to perform primer-independent replication that results in the synthesis of a full-length copy of the genome template.

The first 11 nucleotides located at the extreme termini of all three LACV segments are strictly conserved and have been shown to form independent RNA secondary structures that interact with the RdRp at separate sites (19). For BUNV, segment-specific nucleotides at subsequent positions 12 to 15 are required to form canonical Watson-Crick base-pairing with corresponding nucleotides at the opposite end of the template (10, 20, 21), and together, these RdRp-RNA and RNA-RNA interactions are proposed to

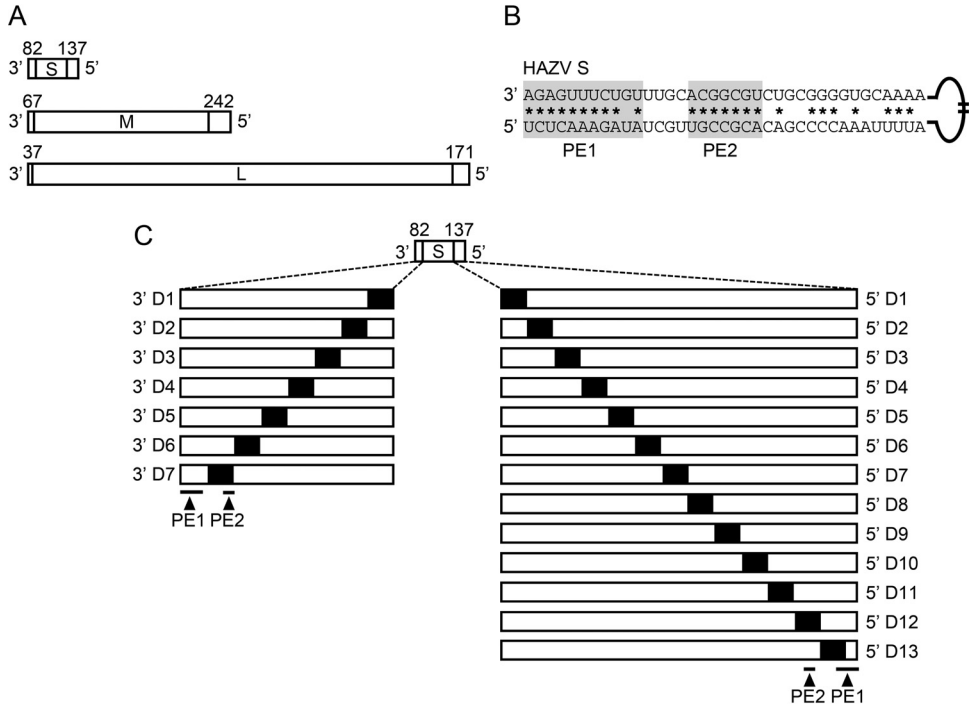

FIG 1 Schematic showing nairovirus S, M, and L segments, the proposed S segment promoter structure, and deletions made within S segment NTRs for attempted rescue. (A) Schematic of HAZV S, M, and L genome segments, with lengths of the respective NTRs shown. (B) Nucleotide sequences of the first 40 terminus-proximal nucleotides of 3′ and 5′ NTRs of the HAZV S segment genome, with termini aligned and with complementary nucleotides marked with an asterisk. Proposed promoter elements PE1 and PE2, comprising complementary nucleotides from both 3′ and 5′ NTRs, are in shaded boxes. (C) Shaded regions represent successive 10-nucleotide-long blocks that were deleted in corresponding S segments and subsequently used to attempt virus rescue with wild-type HAZV M and L segments. Positions of nucleotides included in the proposed PE1 and PE2 regions are shown for reference.

account for the pseudocircular appearance of BUNV and LACV RNPs (22, 23). While sequence changes within the 11 strictly conserved terminal proximal nucleotides have a profound influence on promoter function, the adjacent nucleotides 12 to 15 are highly tolerant of nucleotide change provided that their interterminal Watson-Crick base-pairing potential is maintained. Just 17 terminal proximal nucleotides from 3′ and 5′ NTRs are required to build up the minimal BUNV transcription and replication promoters (24), and with the exception of a transcription termination signal within the BUNV genomic 5′ NTR (12), roles of the remaining nucleotides in both NTRs are currently unclear. NTR deletion analysis in the context of infectious virus has identified functionally important sequences within the BUNV NTRs, with deletion of some regions leading to growth attenuation or lack of virus viability (13, 16), although their specific roles are currently unknown.

For the nairoviruses, little is known of the roles of the 3′- and 5′-terminal NTRs, either in signaling RNA synthesis or in the broader context of the virus multiplication cycle. As with other *Bunyavirales* members, the NTRs of all nairoviruses comprise highly conserved terminal proximal nucleotides shared by all segments, followed by less conserved regions that are segment specific and extend for between 37 and 82 nucleotides at the genomic 3′ end and 137 to 242 nucleotides at the genomic 5′ end (Fig. 1A). The variation in length between the 3′ and 5′ NTRs across all three segments is striking and raises the possibility that the longer NTRs may contain redundant sequences or, alternatively, may contain signals that confer additional segment-specific properties within the context of the virus replication cycle.

A recent study, the first to define nairovirus NTR functionality, employed HAZV minigenomes to characterize promoter elements (PEs) that are involved in the signaling of reporter activity as a marker for RNA synthesis (25); PE1 comprised strictly conserved

3′ and 5′ terminus-proximal sequences, whereas PE2 comprised a GC-rich sequence that was predicted to form interterminal Watson-Crick pairings, similar to that described previously for BUNV (10, 20). PE1 and PE2 were found to be separated by a spacer region, which exhibited a critical requirement for short length and lack of base-pairing ability (Fig. 1B).

We recently reported the establishment of a reverse genetics system for HAZV with the ability to efficiently generate infectious HAZV from recombinant sources (26). This system represents a valuable tool with which to better understand the HAZV multiplication cycle and, by extrapolation, that of other nairoviruses, including those requiring high-level containment facilities for their study. Here, we describe the first mutagenic analysis of the 3′ and 5′ NTRs of the HAZV S segment in the context of infectious virus. Our intention was to identify both dispensable and critical sequences in the NTRs in order to better understand their roles in promoting HAZV multiplication throughout the infectious cycle. A total of 26 recombinant HAZV variants with deletions of successive blocks of 3′ and 5′ S segment NTR sequences were constructed, and analysis of growth of the resulting rescued viruses identified several sequences that impacted virus growth and infectivity and confirmed the requirement of potential interterminal base-pairing within PE2 for efficient gene expression.

RESULTS

Mutagenesis strategy to identify NTR sequences critical for virus viability. To assess the roles of both 3′ and 5′ NTRs in the HAZV multiplication cycle, we exploited our recently reported three-plasmid system for the rescue of infectious HAZV (strain JC280), in which expression of S, M, and L antigenomic RNAs was driven by bacteriophage T7 RNA polymerase (RNAP) in hamster-origin BSRT7 cells (26). Transfection of these plasmids into cells allowed transcription and translation of S, M, and L antigenomes followed by assembly of HAZV RNPs and subsequent generation of infectious HAZV. An additional plasmid to express exogenous T7 RNAP was also included, which increased rescue efficiency.

Our strategy for this study was to generate mutant infectious viruses bearing successive deletions of 10 nucleotides throughout both S segment 3′ and 5′ NTRs, defined here as comprising 3′ nucleotides upstream and excluding the start codon, and comprising 5′ nucleotides downstream and excluding the stop codon, and to examine their growth and infectivity in BSRT7 and human-origin SW13 cells. We chose to perform this analysis using the HAZV S segment due to the small size of its corresponding NTRs and consequent ease of mutagenesis. A consistent deletion size of 10 nucleotides was chosen to allow both NTRs to be covered by a manageable number of mutant viruses and to provide a sufficiently large deletion window that would increase the likelihood of ablating any critical signals.

A total of seven 3′ NTR deletions and 13 5′ NTR deletions were individually engineered into the corresponding S segment plasmid (Fig. 1C), with the changes spanning the entire 3′ and 5′ NTRs and including the previously described PE1 and PE2 (25). Plasmids were named 3′D1 to 3′D7 and 5′D1 to 5′D13, accordingly (Fig. 1C), and the full 3′ and 5′ NTR sequences of all corresponding mutants are shown in Fig. S1A and S1B, respectively.

Examining the role of 3′ NTR sequences in HAZV multiplication. The seven altered plasmids expressing 3′ S segment NTR deletions 3′D1 to 3′D7 were individually transfected into BSRT7 cells along with wild-type (WT) HAZV M- and L-expressing plasmids to attempt virus rescue. Successful rescue was determined by observing an increase in HAZV N protein abundance in 5-day-posttransfection (dpt) cell lysates compared to control transfections in which the L segment expression plasmid was omitted, measured by Western blot analysis (Fig. 2A). For all attempted virus rescue experiments, 5-dpt supernatants were collected and titers of all rescued viruses calculated by plaque assay on human-origin SW13 cells (Fig. 2B and C). This analysis provided a measure of virus fitness, with supernatant titers consistently correlating with subsequent measure of virus growth. For the most severely attenuated viruses, plaque

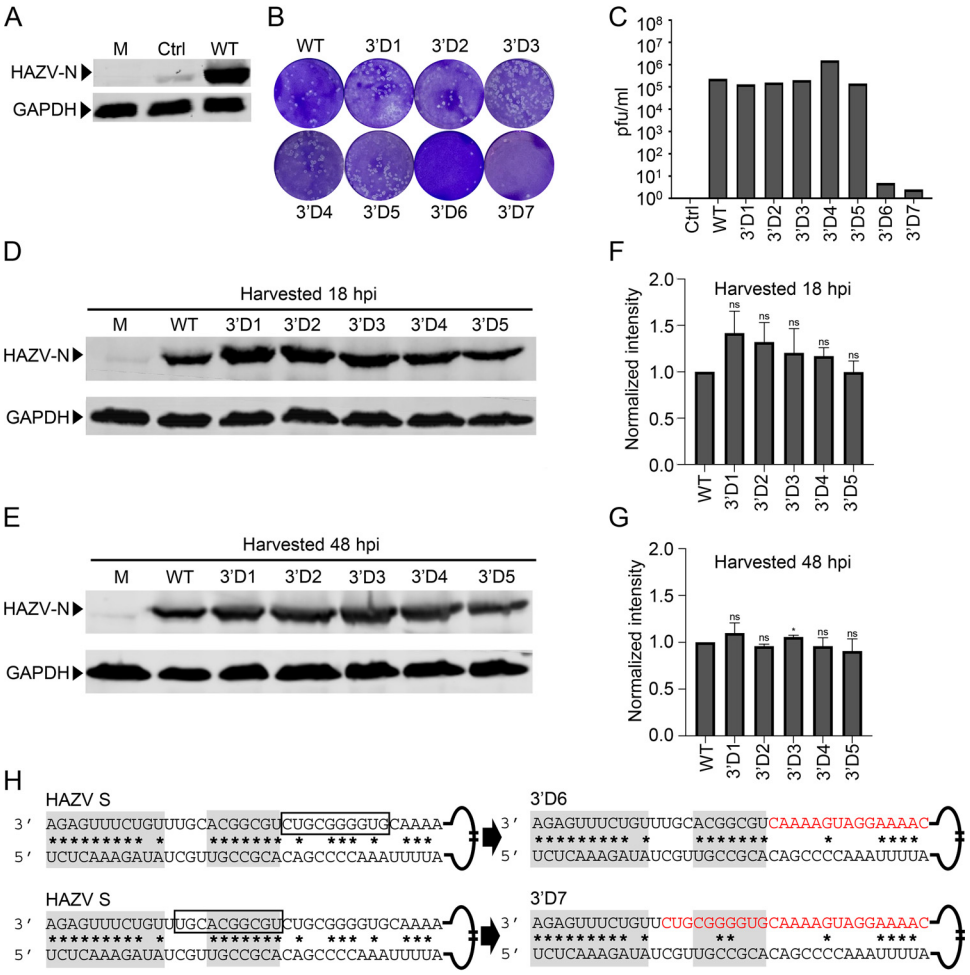

FIG 2 Rescue of recombinant HAZV with S segments bearing successive 10-nucleotide deletions in the 3′ NTR. (A) Successful rescue of recombinant wild-type HAZV from cDNAs expressing S, M, and L segments, as indicated by Western blot analysis of transfected BSRT7 cell lysates using HAZV N protein antisera. M (mock), untransfected lysates; Ctrl (control), transfected cells in which the L segment-expressing cDNA was omitted. (B) Crystal violet-stained plaque assay to determine titers of rescued recombinant viruses from initial transfection cultures, with a single well of each 3′ NTR deletion mutant shown (not equivalent dilutions). (C) Resulting titers. (D and E) Growth properties of mutant viruses bearing 3′ NTR deletions, as determined by Western blot analysis using HAZV N protein antisera of SW13 cultures infected at an MOI of 0.01. Lysates were harvested at 18 hpi (D) and 48 hpi (E). (F and G) Corresponding N protein abundance, determined by densitometry analysis of three independent infections. One sample *t* test was performed to determine statistically significant differences between mutants and WT virus. ns, not significant; *, $P < 0.1$. (H) Nucleotide alignment of genomic 3′ and 5′ NTRs of the highly attenuated mutants 3′D6 and 3′D7, with complementary nucleotides marked with an asterisk and PE1 and PE2 promoter elements in shaded boxes. Open boxes show deleted nucleotides, and red nucleotides show subsequent alterations in the context of the terminal duplex.

assay analysis of rescue supernatants also provided a confirmation of viability and allowed examination of plaque size and morphology as an alternative means to assess virus growth properties.

The HAZV mutants 3′D1 to 3′D7 were rescued on the first attempt, and with the exception of 3′D7, genotypes were confirmed by sequence analysis of reverse transcription-PCR (RT-PCR) products spanning the intended sequence changes. Plaque assay analysis revealed that mutants 3′D1 to 3′D5 were rescued and subsequently multiplied to posttransfection supernatant titers similar to those of WT HAZV, which was rescued concurrently (Fig. 2B and C). Measurement of plaque size as an additional assessment of virus growth characteristics revealed no significant variation, and plaque morphology was consistent, displaying the characteristic dark center previously referred to as a "bulls-eye" plaque (27). In contrast, for mutants 3′D6 and 3′D7, SW13 cell

plaque assay of 5-dpt supernatants revealed titers of around 10 viruses per ml, suggesting that while these viruses were viable, they were extremely unfit (Fig. 2B and C). Repeated transfections confirmed these observations, with equivalent titers obtained on subsequent occasions.

The growth characteristics of mutant viruses were measured by infecting SW13 cell cultures at a multiplicity of infection (MOI) of 0.01 and assessing N protein production as a surrogate marker for HAZV gene expression by Western blotting at both 18 and 48 h postinfection (hpi) (Fig. 2D and E). N abundance at 18 hpi represented N production in a single step of virus multiplication in initially infected cells, whereas the 48-hpi time point also measured the ability of the mutant viruses to assemble and reinfect further cells within the culture. N protein abundance was quantified by densitometry from three independent infections for each mutant used (Fig. 2F and G). The titers of mutants 3′D6 and 3′D7 were too low to permit infection at an MOI of 0.01, and even in infections using undiluted titrated supernatants (MOI, approximately 2×10^{-5}), N protein was not reliably detected at the 18-hpi time point of single-step growth. Comparison between N protein production of mutants 3′D1 to 3′D5 and that of the WT revealed that deletion of any of the associated nucleotides has no major impact on virus growth, with no significant differences in N protein abundance at either 18- or 48-hpi time points, with the exception of 3′D3, for which a difference of minor significance was recorded.

Examination of the resulting nucleotide sequence of the low-viability mutant 3′D6 revealed that the changes did not impinge on either PE1 or PE2 (Fig. 2H, top), thus revealing a critical role in HAZV viability for residues outside the established PE1 and PE2 regions. For mutant 3′D7, in which the entire PE2 region was deleted (Fig. 2H, bottom), its barely detectable multiplication also indicates that the PE2 region is required for efficient HAZV multiplication, corroborating and extending previous work by others (25) that concluded that the analogous M segment PE2 was required for minigenome reporter expression.

Examining the role of 5′ NTR sequences in HAZV multiplication. The strategy used to attempt rescue of the 13 5′ NTR mutants was identical to that used for 3′ NTR mutants, described above. Recombinant mutant viruses 5′D1 to 5′D11 were rescued on the first attempt, and observation of resulting plaques (Fig. 3A) revealed no detectable differences in plaque size or morphology compared to WT. Titers of rescued viruses in posttransfection supernatants were determined (Fig. 3B), and all fell within 1 log of that of WT HAZV, rescued concurrently. In contrast, viruses 5′D12 and 5′D13 failed to rescue on the first attempt, and following further failed attempts, rescue was deemed unattainable.

The growth characteristics of 5′ NTR mutant viruses 5′D1 to 5′D11 were measured by infecting SW13 cell cultures at an MOI of 0.01 and assessing N protein production as a surrogate marker for HAZV gene expression by Western blotting at both 18 and 48 hpi (Fig. 3C and D). At the 18-hpi time point, representing a single infectious cycle, rescued viruses 5′D3 to 5′D7 exhibited significantly reduced N protein expression compared to the WT, as quantified by densitometry of three independent infections (Fig. 3E and F). This suggested that these viruses possessed a deficiency in an early stage of the life cycle, up to and including S segment mRNA accumulation and subsequent N protein translation. At the 48-hpi time point, the same viruses with the exception of 5′D4 and 5′D5 still showed reduced N production compared to the WT, suggesting that the influence of the deficiency was maintained through subsequent rounds of infection.

The nucleotide alterations in mutants 5′D13 and 5′D12, which failed to rescue, impinge upon PE1 and PE2, respectively, which confirms the critical role of these S segment sequences in the HAZV multiplication cycle. In addition, the significant drop in virus growth for the viruses 5′D3 to 5′D7 revealed important roles for the corresponding 50 deleted nucleotides, which together represent almost half of the entire 5′ NTR.

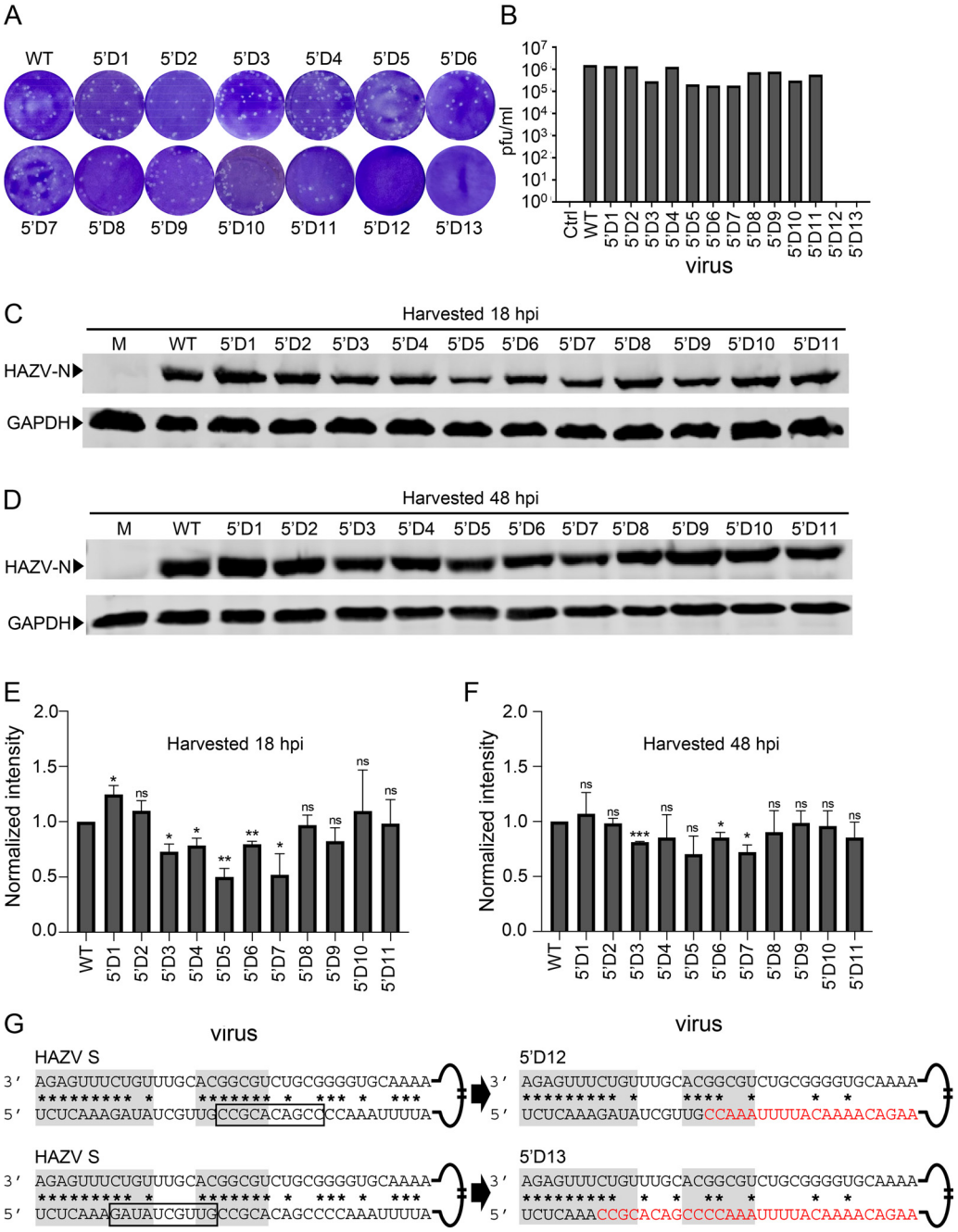

FIG 3 Rescue of recombinant HAZV with S segments bearing successive 10-nucleotide deletions in the 5′ NTR. (A) Crystal violet-stained plaque assay to determine titers of rescued recombinant viruses from initial transfection cultures, with a single well of each 5′ NTR deletion mutant shown (not equivalent dilutions). (B) Resulting virus titers. (C and D) Growth properties of mutant viruses bearing 5′ NTR deletions as determined by Western blot analysis using HAZV N protein antisera of SW13 cultures infected at an MOI of 0.01. Lysates were harvested at 18 hpi (C) and 48 hpi (D). (E and F) Corresponding N protein abundances determined by densitometric analysis of Western blots representing three independent infections. One sample *t* test was performed to determine statistically significant differences between mutants and WT virus. ns, not significant; *, $P < 0.1$; **, $P < 0.01$; ***, $P < 0.001$. (G) Nucleotide alignment of genomic 3′ and 5′ NTRs of highly attenuated mutants 5′D12 and 5′D13, with complementary nucleotides marked with an asterisk and PE1 and PE2 promoter elements in shaded boxes. Open boxes show nucleotides to be deleted, and red nucleotides show subsequent alterations in the context of the terminal duplex.

Taken together, these results show that any impingement on PE1 and PE2 within either 3′ or 5′ NTRs represents a severely debilitating or even lethal mutation, and the 5′ NTR is more sensitive to alteration that the 3′ NTR, likely due to the presence of functionally important sequences within this region.

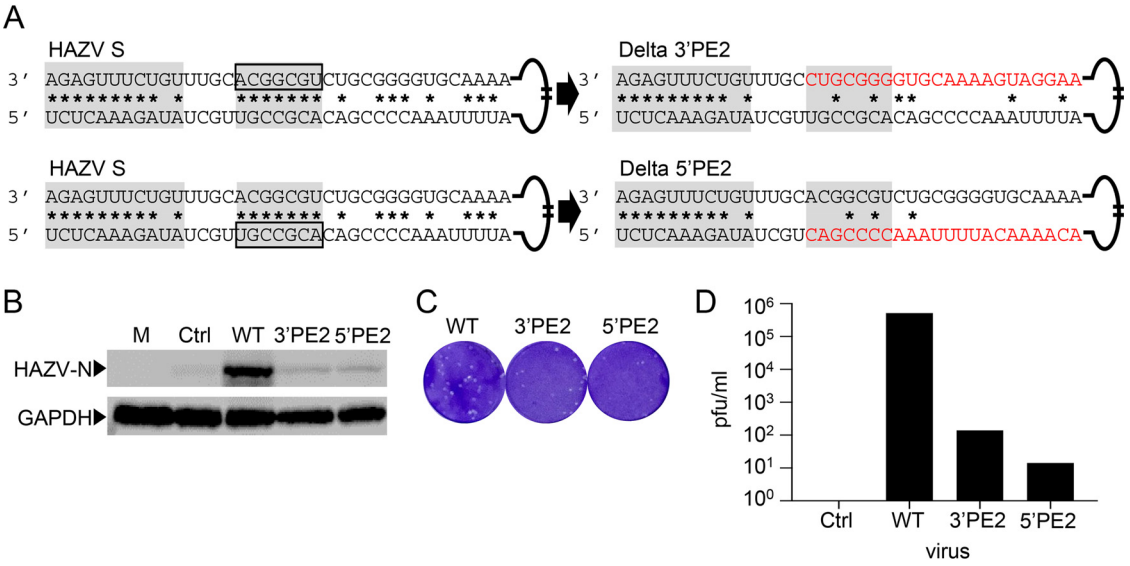

FIG 4 Effect of deletion of S segment PE2 on HAZV viability. (A) Nucleotide sequence alignment of genomic 3′ and 5′ NTRs of wild-type and mutant HAZV S segments bearing changes within PE2, with complementary nucleotides marked with an asterisk and PE1 and PE2 promoter elements in shaded boxes. Open boxes show nucleotides to be deleted, and red nucleotides show subsequent alterations in the context of the terminal duplex. (B) Successful rescue of recombinant HAZV, indicated by Western blot analysis of transfected-cell lysates using HAZV N protein antisera. M (mock), untransfected lysates; Ctrl (control), transfected cells in which the L segment-expressing cDNA was omitted. (C) Crystal violet-stained plaque assay to determine titers of rescued recombinant Delta 3′PE2 and Delta 5′PE2 viruses from initial transfection cultures, alongside the wild type, with a single well of both viruses shown (not equivalent dilutions). (D) Resulting titers.

The importance of PE2 nucleotide composition for virus viability. The results described above showed that mutants 3′D6 and 3′D7 were viable but extremely unfit, and mutants 5′D12 and 5′D13 could not be rescued. Interestingly, for mutants 3′D7, 5′D12, and 5′D13, the altered nucleotides fall within PE2, the terminal-distal promoter region found to require, in major part, interterminal Watson-Crick base-pairing for its promoter activity (25). The number of potential complementary interterminal pairings within these three mutants differs; for 3′D7 it is just two (Fig. 2H), for 5′D12 it is five (Fig. 3G), and for 5′D13 it is three (Fig. 3G). Taken together, these findings are consistent with the proposal that a high degree of complementarity within PE2 is an important determinant of virus viability.

To further investigate the role of PE2 nucleotides during the complete HAZV infectious cycle, we designed plasmids to generate altered S segments in which the entire seven nucleotides that correspond to either 3′ or 5′ components of PE2 were cleanly deleted, yielding plasmids Delta 3′PE2 and Delta 5′PE2, respectively (Fig. 4A). The alterations reduced the number of potential interterminal base pairs within the proposed PE2 region from seven to just two, and based on the finding that mutants 3′D7, 5′D12, and 5′D13 bearing partially deleted PE2 regions were either barely viable or nonviable, we predicted that Delta 3′PE2 and Delta 5′PE2 would be similarly unfit or nonviable.

The corresponding altered plasmids were transfected into cells to attempt rescue, and although rescue of Delta 3′PE2 and Delta 5′PE2 was achieved (Fig. 4B), their resulting titers were extremely low (Fig. 4C), fewer than 200 viruses per ml in transfected-cell supernatants (Fig. 4D). This outcome was entirely consistent with the proposed important role of nucleotide complementarity in the functionality of PE2 but nevertheless showed that extensive complementarity was not an absolute necessity for virus viability.

To further test the contribution of nucleotide sequence identity to the functionality of PE2, we next designed plasmid G/C PE2 to generate an S segment in which the overall interterminal complementarity of PE2 was unchanged, comprising two A-U pairings and five G-C pairings, but which possessed a novel sequence that was not present in WT S, M, or L segments (Fig. 5A). The plasmid was transfected into cells, and

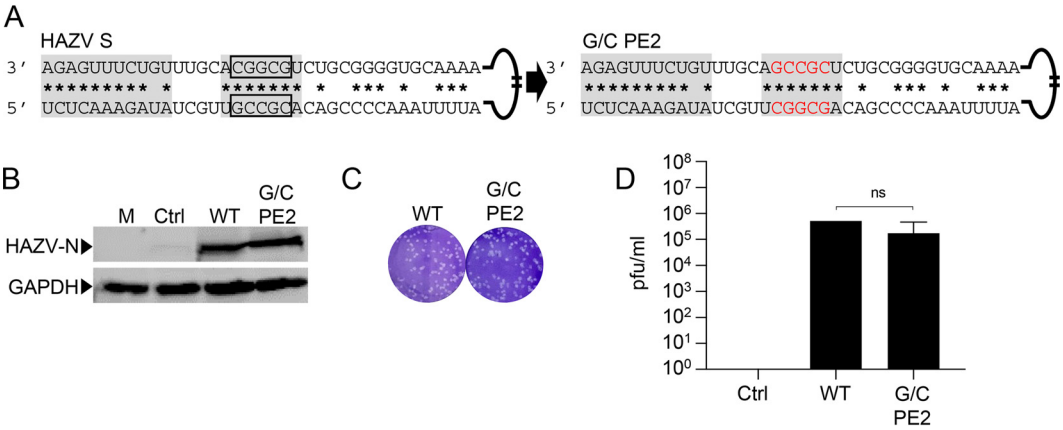

FIG 5 Nucleotide complementarity of PE2 is a key determinant of HAZV viability. (A) Nucleotide sequence alignment of genomic 3′ and 5′ NTRs of wild-type and G/C mutant S segments, with complementary nucleotides marked with an asterisk and PE1 and PE2 promoter elements in shaded boxes. Open boxes show nucleotides to be deleted, and red nucleotides show subsequent alterations in the context of the terminal duplex. (B) Successful rescue of the recombinant HAZV G/C mutant, indicated by Western blot analysis of transfected-cell lysates using HAZV N protein antisera. M (mock), untransfected lysates; Ctrl (control), transfected cells in which the L segment-expressing cDNA was omitted. (C) Crystal violet-stained plaque assay to determine titers of rescued recombinant G/C HAZV from initial transfection cultures alongside the wild type, with a single well of both viruses shown (equivalent dilutions). (D) Resulting mean titers from two independent rescue experiments. A paired *t* test was performed to determine statistically significant differences between mutant and WT virus. ns, not significant.

the corresponding virus G/C PE2 was rescued at the first attempt (Fig. 5B). Plaque assay of the resulting supernatants revealed growth characteristics that were indistinguishable from those of WT virus that had been rescued alongside (Fig. 5C and D). Taken together, these findings are consistent with a scenario in which the base-pairing potential of PE2 is important rather than absolutely necessary and furthermore does not depend on specific sequence.

PE2 represents an independent and modular *cis*-acting sequence signal. Our findings described above, and those of previous studies (25), highlight the importance of PE2 and also show that its signaling ability can be provided by multiple different sequences. Taken together, these results suggest that PE2 acts as an independent module that provides its signaling ability without interaction with PE1 or any other sequence signals elsewhere within the NTRs.

To test the independent signaling ability of PE2 in the context of the complete HAZV replication cycle, we generated an S segment plasmid in which both 3′ and 5′ portions of the M segment PE2 (Fig. 6A) replaced the corresponding sequences of the S segment (Fig. 6B). This strategy allowed us to switch sequences that were entirely wild type and thus known to be functional in their respective segment contexts. The resulting virus would thus possess an M segment PE2 surrounded by all other control sequences derived from the S segment.

The M-PE2 plasmid along with WT M and L segment-expressing plasmids were transfected into BSRT7 cells, and virus was recovered at the first attempt (Fig. 6C), with a supernatant titer not significantly different from that of the WT, indicating a high level of virus fitness (Fig. 6D and E). This finding indicated that PE2 could be interchanged and still remain functional in an entirely different sequence context, thus implying that the signaling ability of PE2 was independent of all other signaling nucleotides. Not surprisingly, viruses in which S segment PE2 nucleotides from either the 3′ NTR or the 5′ NTR alone were exchanged for the corresponding M segment PE2 sequences (3′M PE2 and 5′M PE2) could not be rescued, further reinforcing the dependence of interterminal interaction within PE2 for its function (Fig. 6C to E).

DISCUSSION

By analogy with other bunyaviruses, the 3′ and 5′ NTRs of nairovirus S, M and L segments are expected to be multifunctional and perform critical functions in signaling

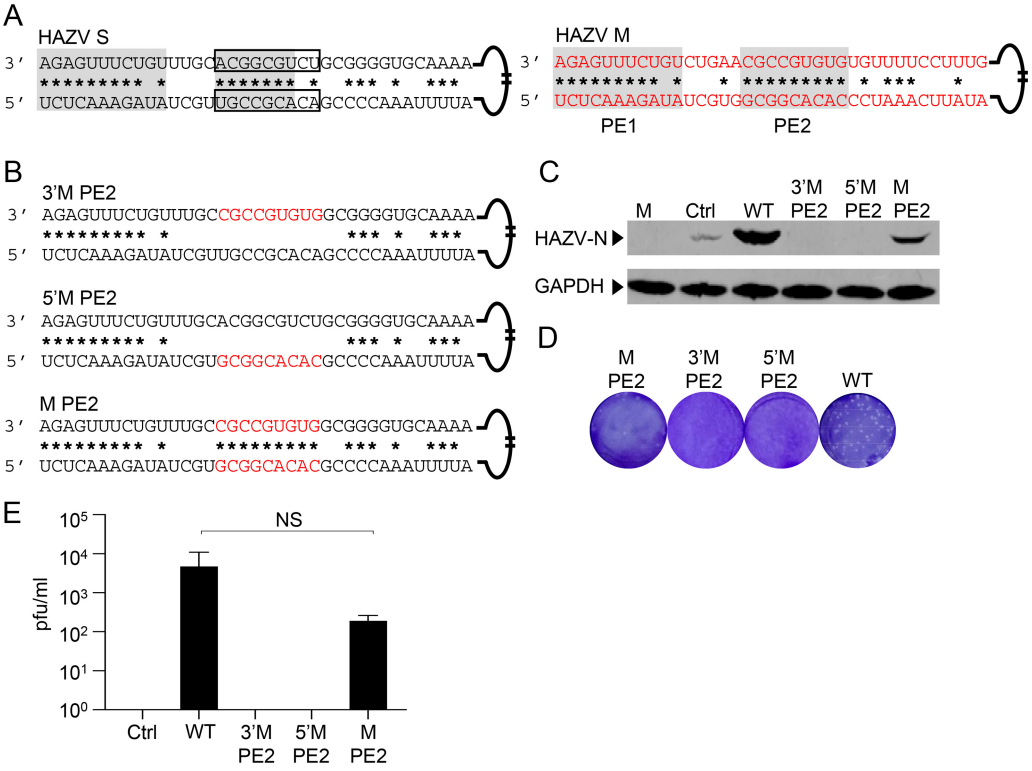

FIG 6 S segment PE2 sequences can be functionally replaced with those of the M segment. (A) Nucleotide sequence alignment of genomic 3′ and 5′ NTRs of HAZV S and M segments, with complementary nucleotides marked with an asterisk and PE1 and PE2 promoter elements in shaded boxes. Open boxes show nucleotides to be deleted. (B) Nucleotide alignment of genomic 3′ and 5′ NTRs of HAZV S segments incorporating M segment PE2 sequences, with M segment-derived nucleotides in red. (C) Successful rescue of recombinant M PE2 indicated by Western blot analysis of transfected-cell lysates using HAZV N protein antisera. M (mock), untransfected lysates; Ctrl (control), transfected cells in which the L segment-expressing cDNA was omitted. (D) Crystal violet-stained plaque assay to determine titers of rescued recombinant HAZV mutants from initial transfection cultures alongside the wild type, with a single well of both viruses shown (not equivalent dilutions). (E) Resulting titers. A paired *t* test was performed to determine statistically significant differences between mutant and WT virus. NS, not significant.

multiple roles relating to viral RNA synthesis, including transcription initiation, transcription termination, mRNA translation enhancement, and RNA replication. However, it is possible that the NTRs participate in additional functions outside RNA synthesis, for which virus fitness throughout the multiplication cycle must be considered.

Here, we performed for the first time a comprehensive deletion analysis of the entire nairovirus 3′ and 5′ NTRs, as well as a further dissection of the role of a discrete promoter element, PE2, all in the context of the entire nairovirus multiplication cycle. Our results revealed that the 3′ genomic NTR is remarkably tolerant of deletion; we detected no significant drop in rescued-virus titer when deletions were made within the terminal distal 50 nucleotides, as represented by rescued viruses 3′D1 through 3′D5. These nucleotide changes also had no significant influence over virus multiplication at either 18 hpi or 48 hpi, suggesting no detectable involvement in virus multiplication in initially infected cells, and also no influence on the assembly, egress, infectivity, and subsequent multiplication of virus in further infected cells. Interestingly, however, deletions closer to the 3′ genomic termini, as exemplified by mutant viruses 3′D6 and 3′D7, exhibited profound effects on virus fitness, with both these mutants being barely viable and being rescued with posttransfection titers of around 10 viruses per ml. The deletion in mutant 3′D7 was within the previously identified conserved PE2 region, confirming the importance of this sequence element. However, the deletion in 3′D6 was outside any previously identified promoter sequence elements, thus newly identifying critical nucleotides required for efficient virus growth. It is noteworthy that of the 10 nucleotides deleted in the 3′ NTR of 3′D6, five possess the potential to form

interterminal Watson-Crick base-pairings. Interestingly, three of these residues form a contiguous triplet of identical nucleotides, with GGG provided by the 3′ NTR and CCC provided by the corresponding positions in the 5′ NTR; furthermore, this feature is also present in the corresponding location in the M and L segments (GGG/CCC in L; AAA/UUU in M). These results show that the nucleotides that build up promoter regions are complex and comprise more than just PE1, PE2, and the intervening spacer.

In contrast to these findings, deletion analysis of the HAZV 5′ genomic NTR revealed that mutant viruses 5′D3 to 5′D7 were significantly growth impaired, with the corresponding nucleotide sequences encompassing 50 nucleotides in the central region of the 5′ NTR. Growth at 18 hpi was significantly reduced compared to that of the WT, with growth at 48 hpi following the same general trend. This suggested that the influence of all the deleted residues was in virus multiplication rather than virion assembly, egress, or infectivity. Mutants 5′D12 and 5′D13 could not be rescued, an outcome that was consistent with their corresponding deletions, which impinged on PE1 or PE2.

The reduced fitness and growth of mutants 5′D3 to 5′D7 suggested that the corresponding deleted nucleotides play an important function in the virus multiplication cycle. Interestingly, the correlations we have determined between genome NTR deletion and virus fitness and growth are broadly similar to those observed for BUNV, for which the 3′ genomic NTR also exhibited considerable functional plasticity compared to the more-sensitive 5′ genomic NTR. Taken together, these findings suggest that bunyavirus 5′ NTRs are more functionally critical than the 3′ end, a notion that is supported by the significant differences in 3′ and 5′ NTR lengths across all segments. Perhaps the most striking example of this is the HAZV L segment, for which the 3′ NTR is 37 nucleotides long, whereas the 5′ NTR is nearly five times as long, comprising 171 nucleotides. Bunyaviruses, such as the prototypic BUNV, have been shown to eliminate nucleotides that are not beneficial to virus multiplication (28), and so it is likely that these long 5′ NTRs do possess significant benefit to certain phases of the multiplication cycle, and perhaps in certain hosts. Recent work with the related segmented negative-strand RNA virus influenza virus has uncovered additional roles of the NTRs, including involvement in intersegment interactions during virus assembly and expression of short viral RNAs involved in modulating RdRp activity or in expressing RNAs that antagonize the host cell innate immune response (29–31). The possibility that the long nairoviral NTRs perform similar roles has yet to be investigated, and these studies provide a first step in this analysis by establishing a framework of NTR functionality.

One role described for the bunyavirus 5′ NTR is in signaling the formation of mRNA 3′ ends. For BUNV, the transcription termination signal resides in a central position of the genomic 5′ NTR and comprises the conserved hexanucleotide sequence 3′-GUCG AC-5′ (12), and a similar motif is also proposed to act as a transcription terminator for the related Rift Valley fever phlebovirus (32, 33). In BUNV, the termination sequence is upstream of the mapped mRNA 3′ end (34) and also adjacent to nucleotides that possess the ability to form a stem-loop secondary structure that possesses translation-enhancing properties (14). Alignment of the HAZV S, M, and L segment 5′ NTRs fails to reveal sequences similar to either these bunyavirus-specific termination signals or the common poly(U) tract motif used by nonsegmented negative-sense RNA viruses for 3′ poly(A) addition. Thus, it is entirely possible that nairovirus 3′ mRNA end formation involves a novel mechanism, which utilizes *cis*-acting sequence signals unrelated to those of other related viruses.

Our deletion analyses revealed the importance of the PE2 regions in the HAZV multiplication cycle, with complete or partial deletion of PE2 nucleotides having a significant influence on overall virus fitness and growth, in agreement with previous reporter analysis in the context of mini-genomes (25). Despite this, we showed that viruses with drastic changes to PE2 affecting both sequence and extent of complementarity were still viable and able to perform all aspects of the multiplication cycle, albeit with very poor fitness.

Our findings, along with those of others (25), strongly suggest that the role of PE2 is to drive nothing other than interterminal interactions mediated by canonical Watson-

Crick pairings. Our finding that an alternate GC-rich PE2 sequence, with no commonality to those in S, M, or L segments, is functionally equivalent to that of the WT in all aspects of the multiplication cycle also agrees with this proposal (Fig. 5), as does the ability of the M segment PE2 to function outside its canonical NTR context (Fig. 6). However, it is important to note that Matsumoto and coworkers (25) suggested that the signal provided by PE2 depended not only on duplex formation but also on the nucleotide sequence of this double-stranded region. This conclusion was based on several variations of the PE2 sequence, with some providing low or undetectable reporter activity despite possessing perfect complementarity throughout the PE2 region. This observation prompted the suggestion that the duplex might be recognized by an RNA binding surface that is capable of distinguishing the base composition of PE2, most likely located on the viral RdRp, perhaps to tether the RNP during transitional events required to reposition the 3′ end of the RNA template from the outer RdRp surface into the RdRp active site. While the mutagenic analysis of PE2 performed here is not sufficiently extensive to definitively prove or disprove the question of PE2 sequence specificity, it is intriguing that the PE2 sequence we engineered into the S segment of G/C PE2 (Fig. 5) has no common sequence with the WT S segment except the flanking A-U pairings, previously shown to be dispensable. Therefore, if such a sequence-specific double-stranded-RNA binding site exists, it must also be capable of binding to this novel PE2 sequence within the recombinant HAZV (rHAZV) G/C PE2, and thus, its nucleotide selectivity must be extremely low.

Achieving a detailed understanding of nairovirus molecular virology is very much in its infancy, in part due to the extreme pathogenicity of the constituent members of this group, and hopefully, progress will accelerate with the use of both the recently reported HAZV minigenome (25) and virus rescue systems (26) that are now available and amenable to low-containment-level study.

MATERIALS AND METHODS

Cells and viruses. Baby hamster kidney-derived BSRT7 cells expressing T7 RNAP were maintained in Dulbecco's modified Eagle medium (DMEM) (Sigma-Aldrich) supplemented with 2.5% fetal bovine serum (FBS) (Invitrogen). Human adrenal cortex SW13 cells were maintained in DMEM containing 10% FBS. All media were supplemented with 100 U/ml penicillin and 100 μg/ml streptomycin, and cultures were grown at 37°C under an atmosphere of 5% CO_2.

Plasmids and virus sequences. Plasmids pMK-RQ-S, pMK-RQ-M, and pMK-RQ-L, expressing the S, M, and L segment antigenomic strands of HAZV strain JC280, were generated as previously described (26). We note that the sequence of the S segment used in the recently reported HAZV minigenome system (25) differs from our JC280 sequence by a single nucleotide, at position 25 of the 3′ NTR. Plasmid pCAG-T7pol was a gift from Ian Wickersham (Addgene plasmid no. 59926). Plasmids expressing altered S segments were generated using the Q5 site-directed mutagenesis kit (New England Biolabs) according to the manufacturer's instructions, and all mutant plasmid sequences were confirmed via sequencing (Genewiz).

Virus rescue. The procedure for rescue of wild type and mutant HAZV was described previously (26). Briefly, six-well plates with 1.5×10^5 BSRT7 cells/well in 2 ml DMEM supplemented with 2.5% FBS were transfected 20 to 24 h later with 1.2 μg of pMK-RQ-S, pMK-RQ-M, and pMK-RQ-L and 0.6 μg pCAG-T7pol, using 2.5 μl Mirus TransIT-LT1 transfection reagent (Mirus Bio) per μg of DNA in 200 μl Opti-MEM (Life Technologies). For recovery of HAZV mutants, the WT S segment-specific plasmid was replaced with the corresponding mutant plasmid. For each recovery, a control transfection was set up in which transfection of pMK-RQ-L was omitted. Culture supernatants were collected at 120 h posttransfection. A 200-μl aliquot of the same supernatant was used to determine virus titers following transfection using a standard plaque assay protocol in duplicate. For each rescued virus except 3′D7, 5′D12, and 5′D13, which were severely attenuated, RT-PCR analysis was used to confirm the expected mutant genotype, alongside control PCR amplifications in which RT was omitted.

Virus infections. Cultures of SW13 cells were infected with mutant and wild-type recombinant HAZV at a specified multiplicity of infection (MOI) in serum-free DMEM at 37°C. After 1 h, the inoculum was removed and cells were washed in phosphate-buffered saline (PBS), after which fresh DMEM containing 2.5% FBS, 100 U/ml penicillin, and 100 μg/ml streptomycin was applied for the duration of the infection.

Western blotting. Cell lysates were prepared by washing monolayers in ice-cold PBS followed by incubation in chilled radioimmunoprecipitation assay (RIPA) buffer (150 mM sodium chloride, 1.0% NP-40 alternative, 0.1% sodium dodecyl sulfate [SDS], 50 mM Tris [pH 8.0]) with agitation for 2 min. Cell material was harvested by scraping and transferred to chilled Eppendorf tubes, after which lysates were centrifuged at 20,000 $\times$ *g* for 15 min, and the insoluble fraction was discarded. SDS gel loading buffer supplemented with dithiothreitol (DTT) was added to the supernatant fraction prior to electrophoresis or storage at −20°C. Proteins were separated on 12% SDS-polyacrylamide gels by electrophoresis and

transferred to fluorescence-compatible polyvinylidene difluoride (FL-PVDF) membranes. HAZV-N antiserum generated as previously described was used to detect HAZV-N in combination with fluorescently labeled anti-sheep immunoglobulin secondary antibodies using the LiCor Odyssey Sa infrared imaging system.

Virus titration. Determination of virus titer for assessment of rHAZV rescue growth characteristics was carried out through plaque assay and performed as previously described (26). Briefly, SW13 cells were seeded (2×10^6) into 75-cm^2 flasks and infected 24 h later with wild-type or mutant rHAZV at an MOI of 0.001. Supernatant was collected at various time points, serially diluted, and then used to infect fresh SW13 cells in a 6-well plate. Following virus adsorption, the inoculum was removed and replaced with 1:1 2.5% FBS DMEM and 1.6% methylcellulose. Plates were incubated for a further 6 days prior to fixing with formaldehyde and staining with crystal violet to reveal plaques.

Extraction of viral RNA and RT-PCR. Viral RNA was first extracted from cell-free supernatant using the QIAamp viral RNA kit (Qiagen) and treated with DNase to remove any contaminating DNA prior to further purification using the RNeasy kit (Qiagen). A cDNA copy was generated using ProtoScript II reverse transcriptase (New England Biolabs) according to the manufacturer's instructions alongside a control in which the reverse transcriptase was omitted. PCR amplification of an ~500-bp fragment using primers specific to the HAZV S segment was achieved using the Q5 High Fidelity polymerase (New England Biolabs). PCR product was resolved on a 1% agarose gel containing 0.01% SYBR Safe (Thermo Fisher) and sequenced (Genewiz).

SUPPLEMENTAL MATERIAL

Supplemental material is available online only.

SUPPLEMENTAL FILE 1, PDF file, 0.02 MB.

ACKNOWLEDGMENTS

This work was funded by a Public Health England Ph.D. studentship to J.F. and an EU Marie Skłodowska-Curie Actions (MSCA) Innovative Training Network (ITN) H2020-MSCA-ITN-2016 grant, no. 721367, to B.A.-R. D.F.M. was self-funded.

J.N.B., J.F., and D.F.M. conceptualized the study, J.F., D.F.M., and B.A.-R. performed the experimental investigation, J.N.B. wrote the original draft, and all other authors reviewed and edited the manuscript. J.N.B. supervised the core team, provided management and coordination of activities, and acquired financial support.

REFERENCES

1. Abudurexiti A, Adkins S, Alioto D, Alkhovsky SV, Avšič-Županc T, Ballinger MJ, Bente DA, Beer M, Bergeron É, Blair CD, Briese T, Buchmeier MJ, Burt FJ, Calisher CH, Cháng C, Charrel RN, Choi IR, Clegg JCS, de la Torre JC, de Lamballerie X, Dèng F, Di Serio F, Digiaro M, Drebot MA, Duàn X, Ebihara H, Elbeaino T, Ergünay K, Fulhorst CF, Garrison AR, Gāo GF, Gonzalez J-PJ, Groschup MH, Günther S, Haenni A-L, Hall RA, Hepojoki J, Hewson R, Hú Z, Hughes HR, Jonson MG, Junglen S, Klempa B, Klingström J, Kòu C, Laenen L, Lambert AJ, Langevin SA, Liu D, Lukashevich IS, Luò T, Lü C, Maes P, de Souza WM, Marklewitz M, Martelli GP, Matsuno K, Mielke-Ehret N, Minutolo M, Mirazimi A, Moming A, Mühlbach H-P, Naidu R, Navarro B, Nunes MRT, Palacios G, Papa A, Pauvolid-Corrêa A, Pawęska JT, Qiáo J, Radoshitzky SR, Resende RO, Romanowski V, Sall AA, Salvato MS, Sasaya T, Shěn S, Shí X, Shirako Y, Simmonds P, Sironi M, Song J-W, Spengler JR, Stenglein MD, Sū Z, Sūn S, Táng S, Turina M, Wáng B, Wáng C, Wáng H, Wáng J, Wèi T, Whitfield AE, Zerbini FM, Zhāng J, Zhāng L, Zhāng Y, Zhang Y-Z, Zhāng Y, Zhou X, Zhū L, Kuhn JH. 2019. Taxonomy of the order Bunyavirales: update 2019. Arch Virol 164:1949–1965. https://doi.org/10.1007/s00705-019-04253-6.
2. Davies FG. 1997. Nairobi sheep disease. Parassitologia 39:95–98.
3. Messina JP, Pigott DM, Golding N, Duda KA, Brownstein JS, Weiss DJ, Gibson H, Robinson TP, Gilbert M, William Wint GR, Nuttall PA, Gething PW, Myers MF, George DB, Hay SI. 2015. The global distribution of Crimean-Congo hemorrhagic fever. Trans R Soc Trop Med Hyg 109:503–513. https://doi.org/10.1093/trstmh/trv050.
4. Negredo A, de la Calle-Prieto F, Palencia-Herrejón E, Mora-Rillo M, Astray-Mochales J, Sánchez-Seco MP, Bermejo Lopez E, Menárguez J, Fernández-Cruz A, Sánchez-Artola B, Keough-Delgado E, Ramírez de Arellano E, Lasala F, Milla J, Fraile JL, Ordobás Gavín M, Martinez de la Gándara A, López Perez L, Diaz-Diaz D, López-García MA, Delgado-Jimenez P, Martín-Quirós A, Trigo E, Figueira JC, Manzanares J, Rodriguez-Baena E, Garcia-Comas L, Rodríguez-Fraga O, García-Arenzana N, Fernández-Díaz MV, Cornejo VM, Emmerich P, Schmidt-Chanasit J, Arribas JR, Crimean Congo Hemorrhagic Fever@Madrid Working Group. 2017. Autochthonous Crimean-Congo hemorrhagic fever in Spain. N Engl J Med 377:154–161. https://doi.org/10.1056/NEJMoa1615162.
5. Surtees R, Dowall SD, Shaw A, Armstrong S, Hewson R, Carroll MW, Mankouri J, Edwards TA, Hiscox JA, Barr JN. 2016. Heat shock protein 70 family members interact with Crimean-Congo hemorrhagic fever virus and Hazara virus nucleocapsid proteins and perform a functional role in the nairovirus replication cycle. J Virol 90:9305–9316. https://doi.org/10.1128/JVI.00661-16.
6. Surtees R, Ariza A, Punch EK, Trinh CH, Dowall SD, Hewson R, Hiscox JA, Barr JN, Edwards TA. 2015. The crystal structure of the Hazara virus nucleocapsid protein. BMC Struct Biol 15:24. https://doi.org/10.1186/s12900-015-0051-3.
7. Wang W, Liu X, Wang X, Dong H, Ma C, Wang J, Liu B, Mao Y, Wang Y, Li T, Yang C, Guo Y. 2015. Structural and functional diversity of nairovirus-encoded nucleoproteins. J Virol 89:11740–11749. https://doi.org/10.1128/JVI.01680-15.
8. Barnwal B, Karlberg H, Mirazimi A, Tan Y-J. 2016. The non-structural protein of Crimean-Congo hemorrhagic fever virus disrupts the mitochondrial membrane potential and induces apoptosis. J Biol Chem 291:582–592. https://doi.org/10.1074/jbc.M115.667436.
9. Barr JN, Elliott RM, Dunn EF, Wertz GW. 2003. Segment-specific terminal sequences of Bunyamwera bunyavirus regulate genome replication. Virology 311:326–338. https://doi.org/10.1016/s0042-6822(03)00130-2.
10. Barr JN, Wertz GW. 2004. Bunyamwera bunyavirus RNA synthesis requires cooperation of 3′- and 5′-terminal sequences. J Virol 78:1129–1138. https://doi.org/10.1128/jvi.78.3.1129-1138.2004.
11. Barr JN, Wertz GW. 2005. Role of the conserved nucleotide mismatch within 3′- and 5′-terminal regions of Bunyamwera virus in signaling transcription. J Virol 79:3586–3594. https://doi.org/10.1128/JVI.79.6.3586-3594.2005.
12. Barr JN, Rodgers JW, Wertz GW. 2006. Identification of the Bunyamwera

bunyavirus transcription termination signal. J Gen Virol 87:189–198. https://doi.org/10.1099/vir.0.81355-0.
13. Mazel-Sanchez B, Elliott RM. 2012. Attenuation of Bunyamwera orthobunyavirus replication by targeted mutagenesis of genomic untranslated regions and creation of viable viruses with minimal genome segments. J Virol 86:13672–13678. https://doi.org/10.1128/JVI.02253-12.
14. Blakqori G, van Knippenberg I, Elliott RM. 2009. Bunyamwera orthobunyavirus S-segment untranslated regions mediate poly(A) tail-independent translation. J Virol 83:3637–3646. https://doi.org/10.1128/JVI.02201-08.
15. Kohl A, Lowen AC, Léonard VHJ, Elliott RM. 2006. Genetic elements regulating packaging of the Bunyamwera orthobunyavirus genome. J Gen Virol 87:177–187. https://doi.org/10.1099/vir.0.81227-0.
16. Lowen AC, Elliott RM. 2005. Mutational analyses of the nonconserved sequences in the Bunyamwera orthobunyavirus S segment untranslated regions. J Virol 79:12861–12870. https://doi.org/10.1128/JVI.79.20.12861-12870.2005.
17. Lowen AC, Boyd A, Fazakerley JK, Elliott RM. 2005. Attenuation of bunyavirus replication by rearrangement of viral coding and noncoding sequences. J Virol 79:6940–6946. https://doi.org/10.1128/JVI.79.11.6940-6946.2005.
18. Kohl A, Bridgen A, Dunn E, Barr JN, Elliott RM. 2003. Effects of a point mutation in the 3′ end of the S genome segment of naturally occurring and engineered Bunyamwera viruses. J Gen Virol 84:789–793. https://doi.org/10.1099/vir.0.18963-0.
19. Gerlach P, Malet H, Cusack S, Reguera J. 2015. Structural insights into bunyavirus replication and its regulation by the vRNA promoter. Cell 161:1267–1279. https://doi.org/10.1016/j.cell.2015.05.006.
20. Kohl A, Dunn EF, Lowen AC, Elliott RM. 2004. Complementarity, sequence and structural elements within the 3′ and 5′ non-coding regions of the Bunyamwera orthobunyavirus S segment determine promoter strength. J Gen Virol 85:3269–3278. https://doi.org/10.1099/vir.0.80407-0.
21. Barr JN, Rodgers JW, Wertz GW. 2005. The Bunyamwera virus mRNA transcription signal resides within both the 3′ and the 5′ terminal regions and allows ambisense transcription from a model RNA segment. J Virol 79:12602–12607. https://doi.org/10.1128/JVI.79.19.12602-12607.2005.
22. Ariza A, Tanner SJ, Walter CT, Dent KC, Shepherd DA, Wu W, Matthews SV, Hiscox JA, Green TJ, Luo M, Elliott RM, Fooks AR, Ashcroft AE, Stonehouse NJ, Ranson NA, Barr JN, Edwards TA. 2013. Nucleocapsid protein structures from orthobunyaviruses reveal insight into ribonucleoprotein architecture and RNA polymerization. Nucleic Acids Res 41:5912–5926. https://doi.org/10.1093/nar/gkt268.
23. Reguera J, Malet H, Weber F, Cusack S. 2013. Structural basis for encapsidation of genomic RNA by La Crosse orthobunyavirus nucleoprotein. Proc Natl Acad Sci U S A 110:7246–7251. https://doi.org/10.1073/pnas.1302298110.
24. Mohl B-P, Barr JN. 2009. Investigating the specificity and stoichiometry of RNA binding by the nucleocapsid protein of Bunyamwera virus. RNA 15:391–399. https://doi.org/10.1261/rna.1367209.
25. Matsumoto Y, Ohta K, Kolakofsky D, Nishio M. 2019. A minigenome study of Hazara nairovirus genomic promoters. J Virol 93:e02118-18. https://doi.org/10.1128/JVI.02118-18.
26. Fuller J, Surtees RA, Slack GS, Mankouri J, Hewson R, Barr JN. 2019. Rescue of infectious recombinant Hazara nairovirus from cDNA reveals the nucleocapsid protein DQVD caspase cleavage motif performs an essential role other than cleavage. J Virol 93:e00616-19. https://doi.org/10.1128/JVI.00616-19.
27. Elliott RM, Wilkie ML. 1986. Persistent infection of Aedes albopictus C6/36 cells by Bunyamwera virus. Virology 150:21–32. https://doi.org/10.1016/0042-6822(86)90262-x.
28. Shi X, van Mierlo JT, French A, Elliott RM. 2010. Visualizing the replication cycle of Bunyamwera orthobunyavirus expressing fluorescent protein-tagged Gc glycoprotein. J Virol 84:8460–8469. https://doi.org/10.1128/JVI.00902-10.
29. Dadonaite B, Gilbertson B, Knight ML, Trifkovic S, Rockman S, Laederach A, Brown LE, Fodor E, Bauer D. 2019. The structure of the influenza A virus genome. Nat Microbiol 4:1781–1789. https://doi.org/10.1038/s41564-019-0513-7.
30. te Velthuis AJW, Long JC, Bauer DLV, Fan RLY, Yen H-L, Sharps J, Siegers JY, Killip MJ, French H, Oliva-Martín MJ, Randall RE, de Wit E, van Riel D, Poon LLM, Fodor E. 2018. Mini viral RNAs act as innate immune agonists during influenza virus infection. Nat Microbiol 3:1234–1242. https://doi.org/10.1038/s41564-018-0240-5.
31. Perez JT, Varble A, Sachidanandam R, Zlatev I, Manoharan M, García-Sastre A, TenOever BR. 2010. Influenza A virus-generated small RNAs regulate the switch from transcription to replication. Proc Natl Acad Sci U S A 107:11525–11530. https://doi.org/10.1073/pnas.1001984107.
32. Albariño CG, Bird BH, Nichol ST. 2007. A shared transcription termination signal on negative and ambisense RNA genome segments of Rift Valley fever, sandfly fever Sicilian, and Toscana viruses. J Virol 81:5246–5256. https://doi.org/10.1128/JVI.02778-06.
33. Lara E, Billecocq A, Leger P, Bouloy M. 2011. Characterization of wild-type and alternate transcription termination signals in the Rift Valley fever virus genome. J Virol 85:12134–12145. https://doi.org/10.1128/JVI.05322-11.
34. Jin H, Elliott RM. 1993. Characterization of Bunyamwera virus S RNA that is transcribed and replicated by the L protein expressed from recombinant vaccinia virus. J Virol 67:1396–1404. https://doi.org/10.1128/JVI.67.3.1396-1404.1993.